Int J Mech Mater Des
https://doi.org/10.1007/s10999-019-09445-1

Influence of interfacial bonding conditions on the anti-penetration performance of ceramic/metal composite targets

Ruixia Yao · Fei Su · Ronghai Mao

Received: 26 August 2018 / Accepted: 27 January 2019

Abstract This study analyzes the influence of bonded and unbonded interface conditions on the anti-penetration performance of a ceramic/metal composite target and determines the associated mechanism. The 3D finite element and 3D smoothed particle hydrodynamics simulation results revealed that a bonded ceramic/metal target exhibited better anti-penetration performance than an unbonded target, and the associated mechanism was determined. Notably, the bond strength between the ceramic and metal backplate plays an important role in the formation of the ceramic conoid, and the ceramic conoid that formed in the bonded target effectively consumed the kinetic energy of the projectile, thereby improving the anti-penetration performance of ceramic composite armor. To verify this conclusion, we also compare and analyze the anti-penetration performance of interface bonded and unbonded metal/metal composite targets. The results show that due to the absence of the ceramic conoid, the interfacial bonding conditions have little influence on the anti-penetration performance of a metal/metal composite target.

Keywords Ceramic/metal composite · Ballistic impact · Damage · Bonding conditions · Finite element · Smoothed particle hydrodynamics

R. Yao · F. Su (✉)
School of Aeronautic Science and Engineering, Beihang University, No. 37 Xueyuan Road, Haidian District, Beijing, China
e-mail: sufei@buaa.edu.cn

R. Yao
e-mail: 759494856@qq.com

R. Mao
Aero Engine Corporation of China, CAE, Shanghai, China
e-mail: maoronghai@hotmail.com

1 Introduction

Ceramic materials are widely used in armor because of their low density, high hardness and high strength. Generally, these materials strongly resist compression but weak when subjected to tension, which causes extensive fragmentation due to the tensile waves generated by the compressive waves reflected from free surfaces. These characteristics have led to the development of composite armor with a ceramic-faced plate and metallic backplate since the use of a ceramic plate alone cannot fully realize the anti-penetration advantage of this approach. When a projectile impacts composite armor, the projectile is initially shattered by the hard ceramic. Then, the broken ceramic forms a conoid, which distributes the force over a larger area and reduces the pressure on the backplate. Finally, the metallic backplate easily absorbs the remaining kinetic energy from the projectile and supports the ceramic fragments.

Many researchers have performed analytical, experimental and numerical analyses on ceramic/

Published online: 22 February 2019

metal composite armor impacted by projectiles. In analytical research, four analytical modellings (Florence and Ahrens 1967; Woodward 1990; Den Reijer 1991; Zaera and Sánchez-Gálvez 1998) were proposed by different researchers in order to estimate trends in impact behavior of ceramic/metal composite armors. In experimental research, Madhu et al. (2004) performed depth of penetration (DOP) experiments on alumina ceramics with different thicknesses based on the impact of 12.7 mm armor-piercing (AP) projectiles. The results indicated that a higher purity alumina (99.5%) exhibited better ballistic performance than 95% alumina for any given thickness and projectile velocity. Übeyli et al. (2008) conducted an experiment using ceramic/aluminum armor and a 7.62 mm AP projectile. The results showed that polyurethane was more effective than epoxy at absorbing the waves generated under impact conditions because of its superior ductility. In numerical research, Lee and Yoo (2001) numerically and experimentally studied the ballistic performance of ceramic/metal composite armor systems using a 2D smoothed particle hydrodynamics (SPH) model. Subramani and Vinoth Kanna (2018) simulated impact behavior of ceramic/metal composite using AUTODYN software, where Johnson–Holmquist model is considered for ceramic materials and Johnson–Cook model is considered for metals. Tepeduzu and Karakuzu (2019) numerically investigated the ballistic behavior of ceramic/composite structures impacted by 7.62 M61 AP projectiles. In his study, 3D models were created and meshed by using LS-DYNA, and Johnson–Holmquist (JH-2) material model was also used for ceramic. Yi et al. (2017) conducted experiments and numerical simulations to study the performance of ceramic composite projectile penetrating into ceramic composite. In their simulation, the Johnson–Holmquist model was also used for brittle material and Johnson–Cook model was also used for metal material.

Some researchers have shown the influence of the adhesive layer on the ballistic performance of composite armor. Grujicic et al. (2012) investigated the role of the adhesive used in ceramic strike-face/composite back-face hybrid armor by transient non-linear dynamics computational finite-element analyses. Tian et al. (2019) found that the additional performance improvement of composite structure derived from the adhesive that bound the ceramic with the frame, the adhesive prolonged the dwell time of the projectile on the ceramic. López-Puente et al. (2005) studied the influence of adhesive layer thickness on the efficiency of lightweight ceramic armors by experimental testing and numerical simulation, and the AUTODYN-2D was also used for numerical simulation. In summary, most numerical studies are based on a simplified 2D finite element analysis and do not clearly explain why the bond strength influences the anti-penetration performance of a ceramic/metal target.

In the current study, several 3D FEM models and 3D SPH models, which are based on DOP tests, are developed using LS-DYNA3D to investigate the influence of different bonding strength of the interface between ceramic and backplate on the anti-penetration performance of ceramic/metal targets, and the associated mechanism is thoroughly discussed.

2 Numerical simulations

In this research, the Hypermesh computer code is used as a preprocessing tool to establish the numerical models. Then, a numerical analysis of penetration is performed using the nonlinear explicit analysis program LS-DYNA3D. The anti-penetration performance of bonded and unbonded ceramic/metal targets impacted by a 12.7 mm AP projectile is numerically simulated with FEM and SPH models. The simulation analysis in this paper is based on the DOP experiments of Madhu et al. (2004).

2.1 FEM model development

In this section, 3D finite element models of the bonded and unbonded ceramic/metal targets impacted by a 12.7 mm hardcore AP projectile are created using Hypermesh and LS-DYNA3D. The bonded and unbonded ceramic/metal targets have the same FEM geometry, material parameters and impact conditions, except that the interface between the two target components (ceramic and backplate) is not allowed to separate (slide) in the bonded case.

For convenient comparisons, a practical projectile-target system with experimental results published by Madhu et al. (2004) was adopted as simulation subject. In this system, the C99.5 ceramics (Al_2O_3 ceramic with purity of 99.5%) backed by two plates of aluminum alloy (Al-7017) is impacted by projectile (see Fig. 1), and the penetration resistance of the

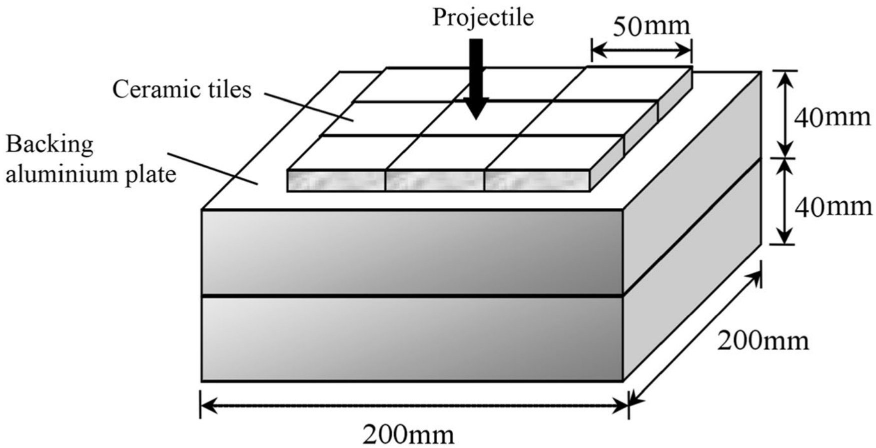

Fig. 1 Schematic diagram of the experiment of projectile-target system (Madhu et al. 2004)

ceramic is evaluated by measuring the DOP (P_{RES}) of the projectile on the metal backplate. The ceramic tile is 50 mm × 50 mm in size with a thickness of 10 mm, and the aluminum backplate is 200 mm × 200 mm in size with a thickness of 40 mm. The hardened steel core of the projectile is covered with a copper sheath and has a diameter of 10.8 mm. The length of the core is 52 mm.

Due to the axisymmetric nature of this situation, only a quarter of the projectile-target system is modeled by the FEM. Corresponding symmetric boundary conditions are applied to the two symmetric surfaces of the projectile-target system, and fixed boundary conditions are applied to the sides of the backplate. All components, including the projectile, ceramic and metal backplate, are modeled with 8-node hexahedron, reduced integration, and hourglass control elements. Since the steel core plays a major role in armor piercing, only the projectile steel core is considered in the simulations. A small radius is introduced at the tip of the hardened steel core to allow a smooth mesh transition. The projectile is divided into 8 elements in the radial direction and 102 elements in the axial direction for a total of 5850 elements. The ceramic is uniformly discretized in a grid of 0.5 × 0.5 × 0.5 mm^3 for a total of 50,000 elements. In addition, transition mesh sizes are adopted for the backplate to reduce the number of grids, resulting in a total of 855,000 elements. The nodes that comprise the projectile grids are assigned an initial velocity of 508 m/s. The finite element model and grids, which contains 910,850 hexahedral elements, are shown in Fig. 2.

The CONTACT_TIED_SURFACE_TO_SURFACE contact algorithm is used to bond the ceramic and backplate in the bonded target to prevent sliding. The contact between the projectile and the target is defined by CONTACT_ERODING_SURFACE_TO_SURFACE, which allows for penetration and perforation by eroding elements from the projectile surface and target. Material failure is controlled by the effective plastic strain in the material constitutive model. If the effective plastic strain reaches a critical value (defined in the material model in LS-DYNA), the element is automatically eliminated from the grids. One-point reduced integration is used in the model along with hourglass control. The LS-DYNA solver calculates the time step using a stability scale factor, which is 0.9 by default. For stability reasons, the scale factor is set to 0.6 to reduce the time step. Various energy changes in the computation are monitored to ensure the stability and credibility of the results.

2.2 SPH model development

To ensure the reliability of the FEM calculation results, we created 3D SPH models of bonded and unbonded ceramic/metal targets impacted by a 12.7 mm hardcore AP projectile. Similar to the finite element models, the only difference between the bonded and unbonded targets in the SPH method is whether the interface between the two target components (ceramic and backplate) was allowed to separate (slide).

SPH is a Lagrangian scheme and gridless technique, and the basic approach is to discretize a part using a cloud of points instead of an ordered mesh

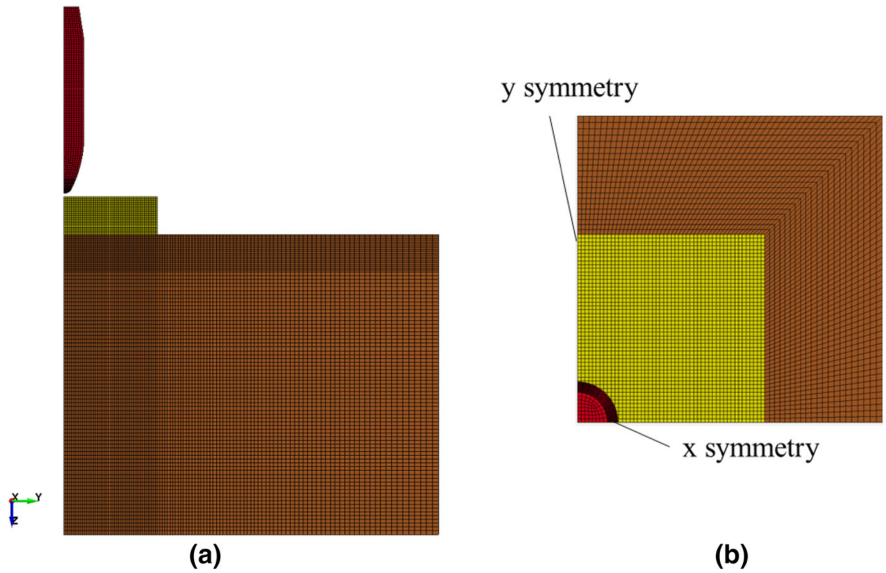

Fig. 2 FEM model of the ceramic/metal target: **a** front view and **b** top view

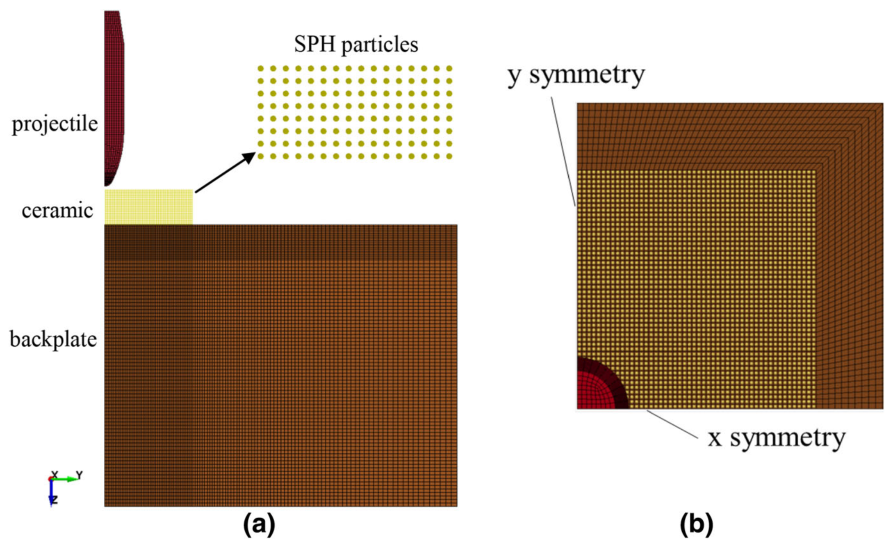

Fig. 3 SPH model of the ceramic/metal target: **a** front view and **b** top view

grid. Using this algorithm prevents the mesh distortion under large deformation but consumes more time than standard element computations. Only a quarter of the projectile-target system is modeled with the SPH method, and only the ceramic is modeled using SPH particles. The projectile and backplate are modeled with the 8-node hexahedron finite elements from the previous section to reduce the calculation time. The ceramic SPH particles are established in the center of each ceramic finite element with a spacing of 0.5 mm for a total of 50,000 SPH particles. The SPH model and particle distribution are shown in Fig. 3, and the model contains 50,000 SPH particles and 860,850 hexahedral grids.

The TIED_NODE_TO_SURFACE is used to define the connection between the backplate and bottom of the ceramic SPH particles in the bonded target to prevent sliding. The interface between the projectile and the ceramic is defined with CONTACT_ERODING_NODE_TO_SURFACE, and the interface between the projectile and the backplate is defined with CONTACT_ERODING_SURFACE_TO_SURFACE. To ensure that the particles do not pass through the symmetry planes, the BOUNDARY_SPH_SYMMTRY_PLANE is defined for the two symmetry planes of the SPH particles. The remaining parameters of the SPH model are the same as those of the FEM model.

2.3 Material model

In the numerical simulation, three different material constitutive models are adopted due to the different material properties of the ceramic, aluminum back-plate and projectile.

The ceramic materials are modeled using the Johnson–Holmquist (JH-2) material model available in LS-DYNA. The JH-2 model parameters for the ceramic materials are given in Table 1 and were obtained from Cronin et al. (2004) and Anderson Jr et al. (1995). The JH-2 model (Johnson and Holmquist 1994, 1999) is applicable for brittle materials subjected to large strains, high strain rate and high pressures, which includes a specific representation of the strength of both intact and fractured material, a pressure–volume relationship that can include bulking, and a damage model that transitions the material from an intact state to a fractured state.

The normalized equivalent stress for the strength is

$$\sigma^* = \sigma_i^* - D(\sigma_i^* - \sigma_f^*) \tag{1}$$

where σ_i^* is the normalized intact equivalent stress, σ_f^* is the normalized fracture stress, and D is the damage ($0 \le D \le 1$).

The normalized equivalent stresses (σ^*, σ_i^*, σ_f^*) have the general form

$$\sigma^* = \frac{\sigma}{\sigma_{\mathrm{HEL}}} \tag{2}$$

where σ is the actual equivalent stress and σ_{HEL} is the equivalent stress at the Hugoniot elastic limit (HEL).

The normalized intact strength ($D = 0$) is given by

$$\sigma_i^* = A(P^* + T^*)^N (1 + C\ln\dot{\varepsilon}^*) \tag{3}$$

The normalized fracture strength ($D = 1$) is given by

$$\sigma_f^* = B(P^*)^M (1 + C\ln\dot{\varepsilon}^*) \tag{4}$$

The normalized pressure is $P^* = P/P_{\mathrm{HEL}}$, where P is the actual pressure and P_{HEL} is the pressure at the HEL. The normalized maximum tensile hydrostatic pressure is $T^* = T/P_{\mathrm{HEL}}$, where T is the maximum tensile hydrostatic pressure the material can withstand. The material constants are A, B, C, M, N and T.

The damage for fracture is accumulated in a manner similar to that used in the Johnson–Cook fracture model. It is expressed as

$$D = \sum \frac{\Delta\bar{\varepsilon}_p}{\varepsilon_p^f} \tag{5}$$

where $\Delta\bar{\varepsilon}_p$ is the equivalent plastic strain during a cycle of integration and ε_p^f is the plastic strain to fracture under a constant pressure P. The specific expression is

$$\varepsilon_p^f = D_1 (P^* + T^*)^{D_2} \tag{6}$$

where D_1 and D_2 are constants and P^* and T^* are as defined previously in Eq. (3).

The hydrostatic pressure, before fracture begins ($D = 0$), is simply

$$P = K_1\mu + K_2\mu^2 + K_3\mu^3 \tag{7}$$

where K_1, K_2 and K_3 are constants and $\mu = \rho/\rho_0 - 1$ for current density ρ and initial density ρ_0.

The projectile is modeled with the Johnson–Cook damage model (Johnson and Cook 1983), which is commonly used to describe the performance of a material under large deformation, high strain rate and high temperature conditions. This model is suitable for

Table 1 JH-2 parameters for the ceramic (Cronin et al. 2004; Anderson Jr et al. 1995)

Density	Elastic constants		Damage constants		Pressure constants			
ρ (kg/m^3)	G (GPa)	K_1 (GPa)	D_1	D_2	K_1 (GPa)	K_2 (GPa)	K_3 (GPa)	β
3700	90.16	130.95	0.005	1	130.95	0	0	1

Strength constants									
HEL (GPa)	P_{HEL} (GPa)	σ_{HEL} (GPa)	μ_{HEL}	T (GPa)	A	B	C	M	N
2.79	1.46	0.005	0.01117	0.2	0.93	0.31	0	0.6	0.6

Table 2 JOHNSON_COOK parameters for the projectile

ρ (kg/m^3)	G (MPa)	A (MPa)	B (MPa)	C	M	N	EPSO	T_m (K)
7850	77	492	310	0.014	1.03	0.27	1.0	1736
T_r (K)	C (J/kg/K)	D_1	D_2–D_5	c (m/s)	S_1	S_2	γ	α
293	477	0.6	0	4569	1.49	0	1.67	0.43

Table 3 PLASTIC_KINEMATIC parameters for the aluminum alloy backplate

ρ (kg/m^3)	E (GPa)	ν	σ_y (MPa)	E_t (MPa)	C	P	f_s
2900	77	0.3	430	700	0	0	0.7

most metal materials. The material properties of the projectile are given in Table 2.

The Johnson–Cook plastic model is defined as

$$\sigma_y = [A + B(\bar{\varepsilon}^p)^N](1 + C \ln \dot{\varepsilon}^*)(1 - T^{*M}) \tag{8}$$

where A, B, C, M, and N are constants. $\bar{\varepsilon}^p$ is the equivalent plastic strain and $\dot{\varepsilon}^* = \bar{\varepsilon}^p / \dot{\varepsilon}_0$ is the plastic strain rate ratio when $\dot{\varepsilon}_0 = 1\text{s}^{-1}$. The equivalent temperature is $T^* = (T - T_r)/(T_m - T_r)$, where T_r is room temperature and T_m is the melting temperature.

The damage factor is expressed as

$$D = \Sigma \frac{\Delta \bar{\varepsilon}^p}{\varepsilon^f} \tag{9}$$

where $\Delta \bar{\varepsilon}^p$ is the equivalent plastic strain. The failure strain ε^f is defined as

$$\varepsilon^f = (D_1 + D_2 \exp D_3 \sigma^*)(1 + D_4 \ln \dot{\varepsilon}^*)(1 + D_5 T^*) \tag{10}$$

where the coefficients D_1–D_5 depend on the material.

The aluminum alloy backplate is modeled with the PLASTIC_KINEMATIC elastic plastic model (Nemat-Nasser 1992). This model is a bilinear elastic plastic model containing formulations that combine isotropic and kinematic hardening. Five material properties (Youngs modulus E, Poissons ratio v, Yield stress σ_y, tangent modulus E_t and hardening parameter β) are required for this material model. The material properties of the aluminum alloy backplate are given in Table 3.

3 Simulation results

Figure 4 shows a series of model results depicting the penetration process of an unbonded ceramic/metal composite target impacted by a 12.7 mm AP projectile with an initial impact velocity of 508 m/s. It can be seen that some of the physical behaviour observed during the penetration process are well captured in the numerical simulation, such as projectile passivation and target erosion.

Figure 5 and Table 4 show the simulation results of the DOP experiments with the bonded and unbonded ceramic/metal targets. The residual penetration (P_{RES}) of the bonded target is much smaller than that of the unbonded target for both the FEM and SPH methods. In the FEM method, the P_{RES} value of the bonded target is 0.4 mm, and P_{RES} of the unbonded target is 10.3 mm. In the SPH method, P_{RES} of the bonded target is 0 mm, and that of the unbonded target is 6 mm. The P_{RES} value of the bonded target in the DOP experiment (Madhu et al. 2004) is 0.2 mm; thus, the numerical simulation results are consistent with those from the DOP experiments. The P_{RES} values for both the bonded and unbonded conditions obtained by the SPH method are slightly smaller than those obtained with the FEM method because the FEM method adopts an "erosion algorithm". In this algorithm, the eroded element has zero stiffness and no resistance to the projectile, while this is not the case in the SPH model. So it is reasonable to conclude that the practical P_{RES} values lie between the two simulated results.

The simulation results in this section show that the interface bonding of the ceramic-faced plate and metal backplate can significantly improve the anti-penetration performance of ceramic/metal armor.

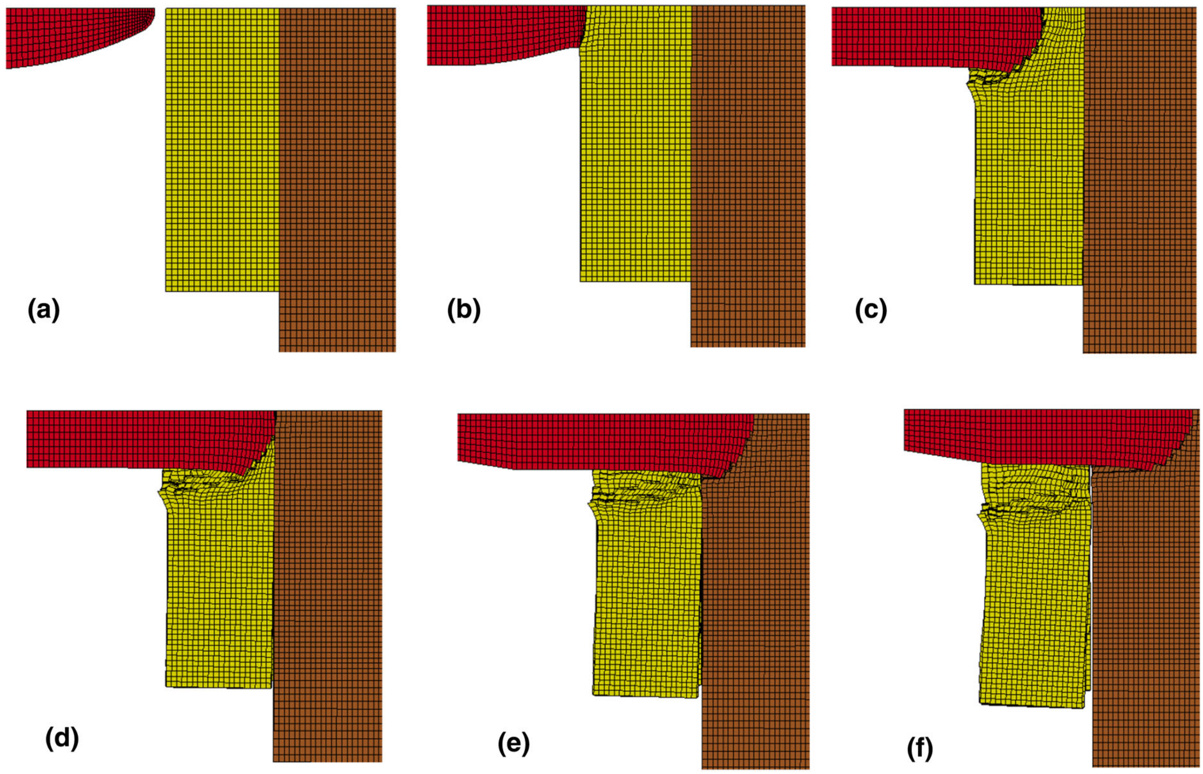

Fig. 4 Penetration process of an unbonded ceramic/metal target impacted by a 12.7 mm projectile at 508 m/s: **a** t = 0 ms, **b** t = 0.015 ms, **c** t = 0.04 ms, **d** t = 0.05 ms, **e** t = 0.08 ms, **f** t = 0.13 ms

4 Discussion and analysis

4.1 Cause of a ceramic conoid

According to stress wave theory, once a projectile impacts a ceramic surface, a compressive stress wave is immediately generated and propagates toward the back of the ceramic (Kaufmann et al. 2003). The ceramic material fractures if the magnitude of the reflected tensile stress wave exceeds the dynamic tensile strength of the material. When the compressive wave propagates to the interface between the ceramic and aluminum backplate, the compressive wave is reflected as a tensile wave because the ceramic wave impedance is greater than that of the metallic backplate. When no adhesion exists between the ceramic and the backplate, the ceramic rapidly breaks into debris and scatters under the impact of a projectile (shown in Fig. 6a). However, when the ceramic and backplate are strongly bonded, the ceramic is only damaged and not shattered (shown in Fig. 6b). Figure 7 reveals the damage (D) evolution process of the ceramic in the bonded target. $D = 0$ represents no damage, and $D = 1$ represents complete damage. Under the combined influence of the compression wave, tensile wave and interfacial bond strength, a conical failure zone forms in the ceramic at 0.35 ms and is called a ceramic conoid (Florence and Ahrens 1967; Woodward 1990; Den Reijer 1991; Zaera and Sánchez-Gálvez 1998).

Figure 8 shows a schematic diagram of a ceramic conoid. According to the analytical ceramic conoid model proposed by Fellows and Barton (1999), the bottom radius of a conoid is

$$R_c = \frac{D_{eq}}{2} + 2h_c$$

where $D_{eq} = \int_0^{L_P} D^3(z)dz \Big/ \int_0^{L_P} D^2(z)dz$ is the equivalent diameter of the projectile ($D(z)$ is the radial position function) and h_c is the thickness of the ceramic.

In this paper, $D_{eq} \approx 10.8$ mm and $h_c = 10$ mm; thus, the theoretical bottom radius of the conoid can be obtained by substituting these values into the above formula.

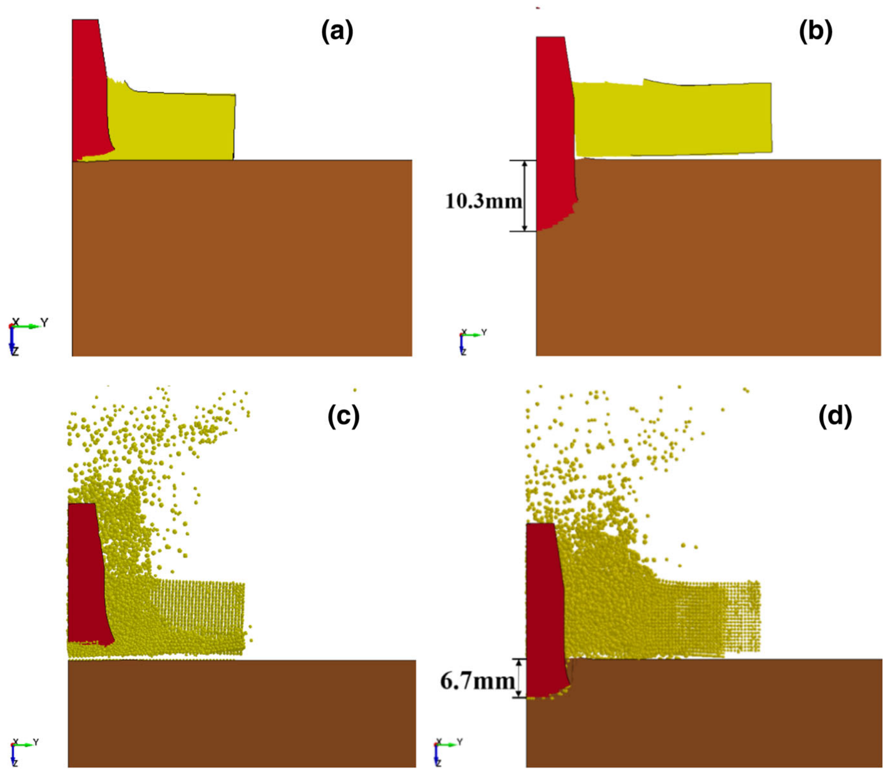

Fig. 5 FEM and SPH simulation results for the bonded and unbonded targets: **a** bonded target (FEM), P_{RES} = 0.4 mm, **b** unbonded target (FEM), P_{RES} = 10.3 mm, **c** bonded target (SPH), P_{RES} = 0 mm, **d** unbonded target (SPH), P_{RES} = 6 mm

Table 4 Comparison of FEM results, SPH results and experimental results

	FEM results	SPH results	Experimental results
Bonded target	0.4 mm	0 mm	0.2 mm
Unbonded target	10.3 mm	6 mm	–

$$R_c = \frac{D_{eq}}{2} + 2h_c = 25.4 \text{ mm} \quad (11)$$

According to the damage contour of the ceramic at 0.035 ms (see Fig. 9), the simulated value of the bottom radius of the ceramic conoid is 23 mm, and the absolute error between the simulated and theoretical values is less than 2.5 mm.

4.2 Reasons for a conoid improving the anti-penetration performance

Figure 10 shows the ceramic resistance to a projectile in the bonded and unbonded ceramic/metal targets throughout the penetration process. Compared to the ceramic in the unbonded target, the ceramic in the bonded targ et has a greater resistance to the projectile and a longer resistance duration. Initially, from 0 to 0.015 ms, the ceramics in the two interfacial bonding conditions have equivalent resistance values for projectiles. In the bonded target, the ceramic resistance to the projectile gradually increases from 0 to 0.035 ms, and the resistance value reaches a maximum of 40 kN at 0.035 ms. Then, the resistance gradually and slowly decreases to 0 at 0.15 ms. However, in the unbonded target, the ceramic resistance to the projectile rapidly decreases after reaching a maximum of 29 kN at 0.03 ms. After 0.075 ms, the ceramic no longer has any resistance to the projectile.

Figure 10 shows that the ceramic resistance to the projectile in both the bonded and unbonded targets reaches a maximum at approximately 0.035 ms and then begins to decline. However, the ceramic resistance to the projectile in the unbonded target rapidly decreases, while that in the bonded target slowly decreases. The slow decrease is because a complete conical structure forms in the ceramic in the bonded target, and this pyramidal ceramic structure still has a considerable resistance to the projectile and consumes

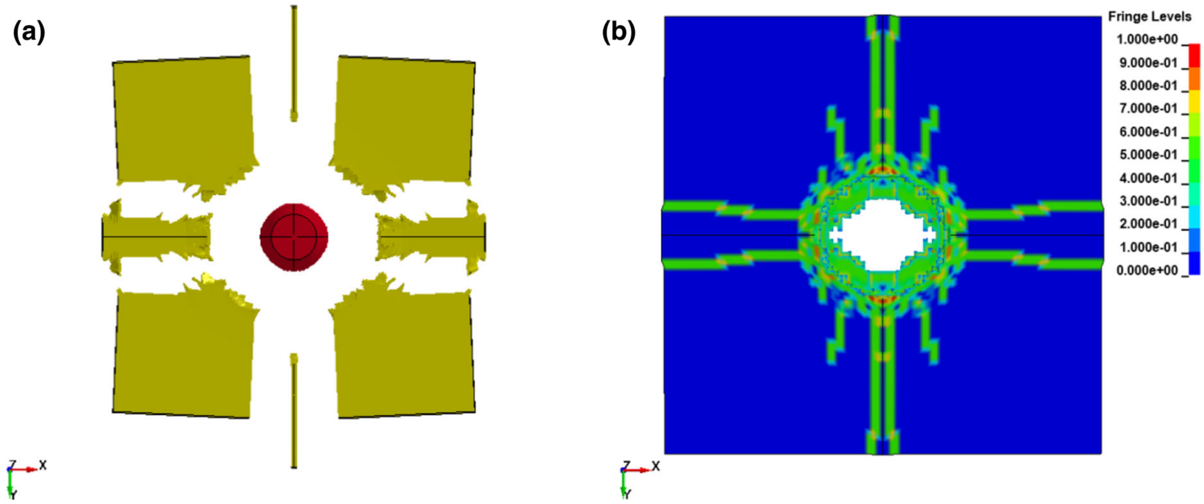

Fig. 6 Different ceramic fracture behaviors: **a** ceramic fracture in the unbonded target, **b** ceramic damage in the bonded target

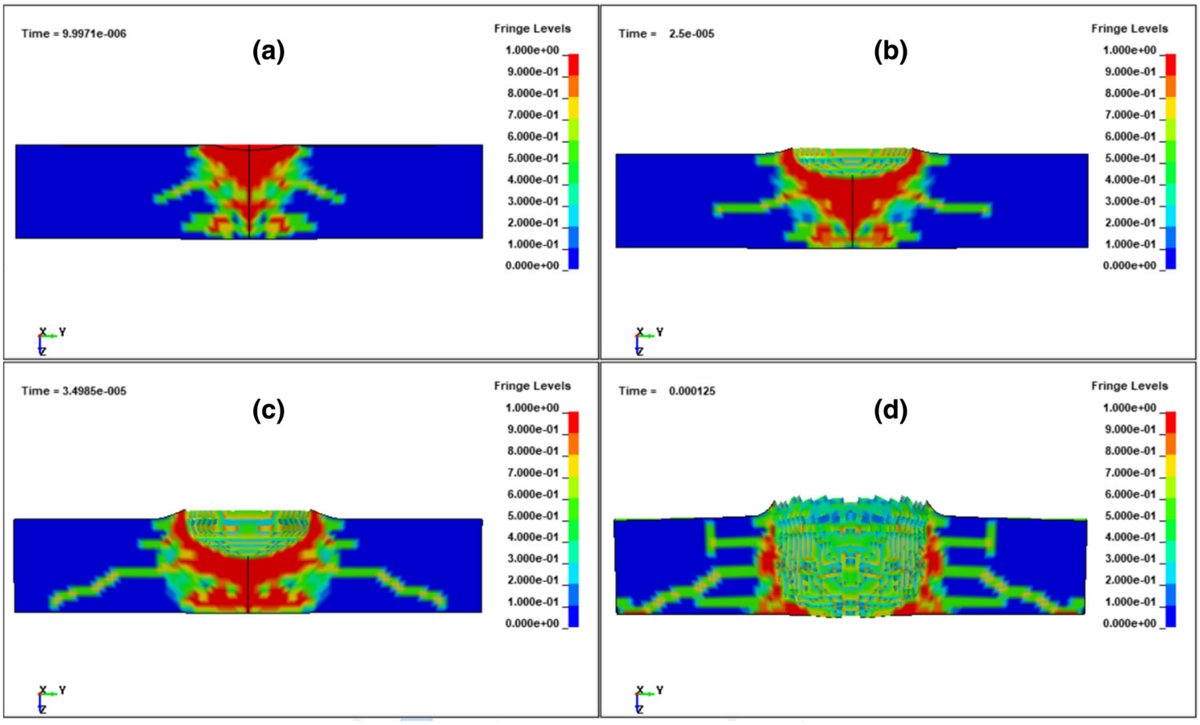

Fig. 7 Damage evolution of the ceramic in the bonded target: **a** t = 0.001 ms, **b** t = 0.025 ms, **c** t = 0.035 ms, **d** t = 0.125 ms

its kinetic energy. Additionally, the projectile impact force is distributed over the base of the conoid, which has an area that is much larger than the projectile cross-section, thereby reducing the pressure on the backplate. However, a ceramic conoid does not form in the unbonded target, and the ceramic shatters and scatters in the initial impact stage. Thus, the ceramic can no longer resist the projectile, and the ceramic resistance to the projectile rapidly decreases.

Figure 11 shows the projectile kinetic energy in the bonded and unbonded target models over time. The projectile kinetic energy is equal for both bonding conditions from 0 to 0.015 ms because of the equal ceramic resistance to the projectile for both bonding conditions during this time (see Fig. 10). Compared with that in the unbonded model, the projectile kinetic energy in the bonded model decreases more quickly because of the greater ceramic resistance to the projectile in the bonded target.

The ceramic conoid that forms in the bonded target can greatly improve the anti-penetration performance of a ceramic/metal composite target, and a sufficiently high bond strength between the ceramic and metal backplate is important for forming the ceramic conoid. In this research, the ceramic conoid forms due to the bonding of the ceramic and backplate, and thus, a bonded target will have a better anti-penetration performance under the impact of a projectile.

For a composite target with a ceramic-faced panel, the interfacial bonding conditions can greatly influence the anti-penetration performance of armor when impacted by projectiles. To further explore this point, variations of DOP with the interface bonding strength of ceramic/metal was simulated and shown in Figs. 12 and 13. The CONTACT_TIEBREAK_NODE_TO_SURFACE contact algorithm was used to connect the ceramic panel and metal backplate for simulating the interface bonding strength. This algorithm allows the application of two failure criteria, namely a maximum

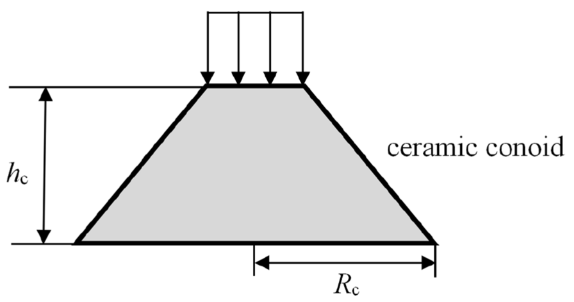

Fig. 8 Schematic diagram of a ceramic conoid (Fellows and Barton 1999)

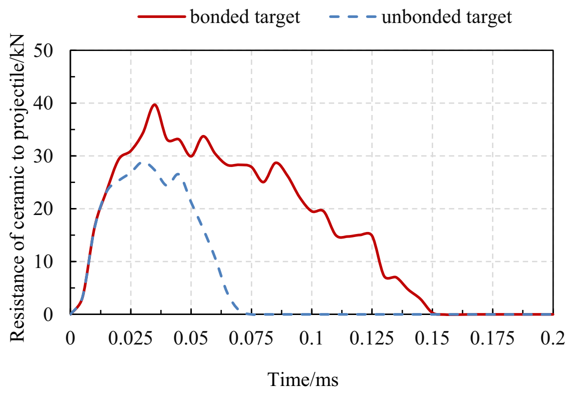

Fig. 10 Ceramic resistance to the projectile over time

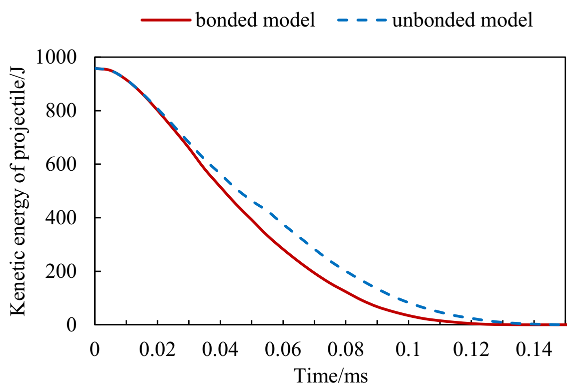

Fig. 11 Projectile kinetic energy versus time

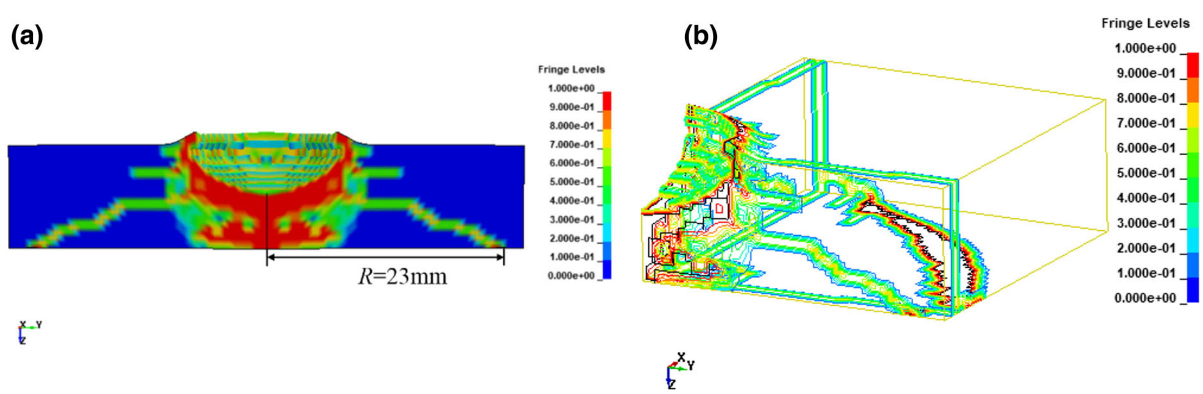

Fig. 9 3D ceramic conoid in the bonded target: **a** bottom radius R = 23 mm, at t = 0.035 ms, **b** ceramic conoid

normal tensile force criterion and a maximum shear force criterion. As can be seen from Figs. 12 and 13, the greater the interface failure force, the smaller the DOP (the closer to 0.4 mm under bonded condition); the smaller the failure force, the greater the DOP (the closer to 10.3 mm under unbonded condition). Therefore, the stronger the bond strength is, the stronger penetration resistance of ceramic composite armor can be.

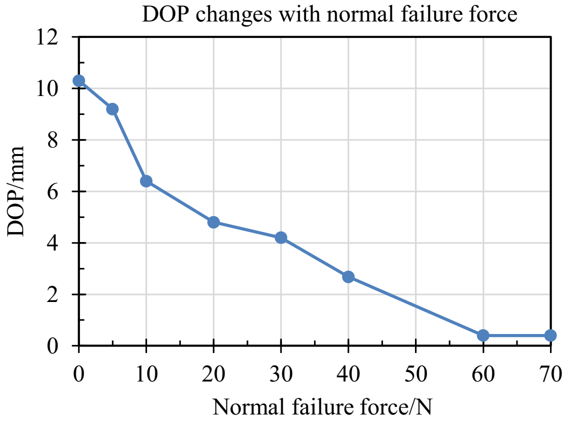

Fig. 12 DOP changes with the normal failure force (no shear failure)

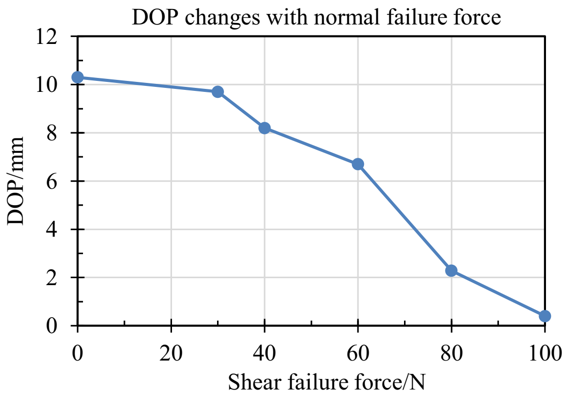

Fig. 13 DOP changes with the shear failure force (no normal failure)

Three-dimensional FEM models of metal/metal targets were also created to analyze the influence of bonded and unbonded interface conditions on the anti-penetration performance of a metal/metal composite target. The ceramic material was changed to a steel material, i.e., a change from a brittle material to a ductile metal, and the DOP simulation results are shown in Fig. 14. The P_{RES} results for the two bonding conditions are both 1.3 mm; thus, little difference exists in the anti-penetration performances of the bonded and unbonded steel/aluminum targets. The results show that for a composite target with a metal-faced panel, the interfacial bonding conditions will minimally influence the anti-penetration performance of the composite armor. However, for a composite target with a ceramic-faced panel, the interfacial bonding conditions can significantly influence the anti-penetration performance of armor when impacted by projectiles.

5 Conclusions

This paper investigated the influence of bonded and unbonded interface conditions on the anti-penetration performance of ceramic/metal composite targets based on both finite element and SPH methods. The results obtained by the two methods all indicate that the bonded target exhibits better anti-penetration performance than the unbonded target because a ceramic conoid forms in the bonded target but not the unbonded target. The conoid can greatly improve the ceramic resistance value and resistance duration

Fig. 14 DOP simulation results for the steel/aluminum target: **a** bonded target, P_{RES} = 1.3 mm, **b** unbonded target, P_{RES} = 1.3 mm

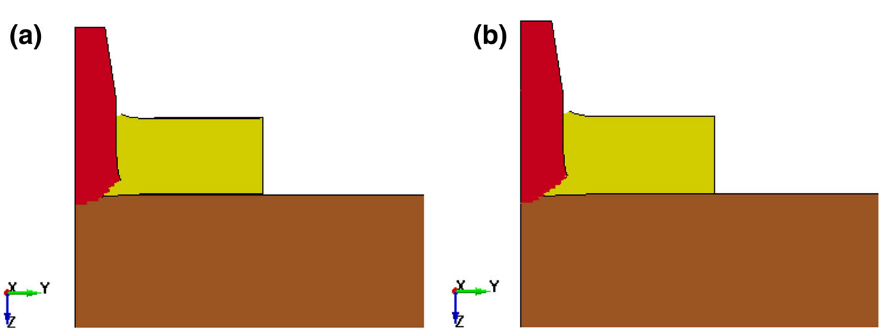

when impacted by a projectile. The 3D ceramic conoid was reproduced in the numerical simulation of the bonded target, and the simulation bottom radius value of the conoid is consistent with the theoretical value. Finally, little difference exists in the anti-penetration performance of a metal/metal target under bonded and unbonded interface conditions. The main conclusions from this study are as follows:

1. For a ceramic/metal composite target with a ceramic-faced panel, a bonded interface can improve the anti-penetration performance.
2. For a metal/metal composite target with a metal-faced panel, the interfacial bonding conditions have little influence on the anti-penetration performance.
3. The bond strength between the ceramic and metal backplate plays an important role in the formation of a ceramic conoid, and the ceramic conoid can greatly improve the anti-penetration performance of a ceramic/metal composite target.

Acknowledgements The authors thank financial support from the National Natural Science Foundation of China (Grant Numbers 11372024 and 11672340).

Compliance with ethical standards

Conflict of interest The authors declare that no conflict of interest exists in the submission of this manuscript.

References

Anderson Jr., C.E., Johnson, G.R., Holmquist, T.J.: Ballistic experiments and computations of confined 99.5% Al_2O_3 ceramic tiles. In: Mayseless, M., Bodner, S.R. (eds.) Proceedings of the 15th International Symposium on Ballistics, vol 2, Jerusalem, Israel, pp. 65–72 (1995)

Cronin, D.S., Bui, K., Kaufmann, C. et al.: Implementation and validation of the Johnson–Holmquist ceramic material model in LS-DYNA. In: Proceedings of the 4th European LS-dyna users conference, vol. 1, pp. 47–60 (2004)

Den Reijer, P.C.: Impact on ceramic faced armour [D]. Delft University of Technology, Delft (1991)

Fellows, N.A., Barton, P.C.: Development of impact model for ceramic-faced semi-infinite armour. Int. J. Impact Eng. **22**(8), 793–811 (1999)

Florence, A.L., Ahrens, T.J.: Interaction of projectiles and composite armor. Final Report, US Army, pp. 135 Ä(1967)

Grujicic, M., Pandurangan, B., D'Entremont, B.: The role of adhesive in the ballistic/structural performance of ceramic/polymer–matrix composite hybrid armor. Mater. Des. **41**, 380–393 (2012)

Johnson, G.R., Cook, W.H.: A constitutive model and data for metals subjected to large strains, high strain rates and high temperatures. In: Proceedings of the 7th International Symposium on Ballistics, pp. 541–547 (1983)

Johnson, G.R., Holmquist, T.J.: An improved computational constitutive model for brittle materials. High pressure science and technology. AIP, New York (1994)

Johnson, G.R., Holmquist, T.J.: Response of boron carbide subjected to large strains, high strain rates and high pressures. J. Appl. Phys. **85**(12), 8060–8073 (1999)

Kaufmann, C., Cronin, D., Worswick, M., et al.: Influence of material properties on the ballistic performance of ceramics for personal body armour. Shock Vib. **10**(1), 51–58 (2003)

Lee, M., Yoo, Y.H.: Analysis of ceramic/metal armour systems. Int. J. Impact Eng. **25**(9), 819–829 (2001)

López-Puente, J., Arias, A., Zaera, R., et al.: The effect of the thickness of the adhesive layer on the ballistic limit of ceramic/metal armours. An experimental and numerical study. Int. J. Impact Eng. **32**(1–4), 321–336 (2005)

Madhu, V., Ramanjaneyulu, K., Bhat, T.B.: An experimental study of penetration resistance of ceramic armour subjected to projectile impact. In: International Symposium on Impact Engineering ISIE (2004)

Nemat-Nasser, S.: Phenomenological theories of elastoplasticity and strain localization at high strain rates. Appl. Mech. Rev. **45**(3S), S19 (1992)

Subramani, K., Vinoth Kanna, I.: Numerical simulation of high velocity impact on composite targets using advanced computational techniques. Innovative Design, Analysis and Development Practices in Aerospace and Automotive Engineering (I-DAD 2018), pp. 399–413. Springer, Singapore (2018)

Tepeduzu, B., Karakuzu, R.: Ballistic performance of ceramic/composite structures. Ceram. Int. **45**(2), 1651–1660 (2019)

Tian, Chao, An, Xuanyi, Sun, Qitian, Dong, Yongxiang: Experimental and numerical analyses of the penetration resistance of ceramic-metal hybrid structures. Compos. Struct. **211**, 264–272 (2019)

Übeyli, M., Yıldırım, R.O., Ögel, B.: Investigation on the ballistic behavior of Al(2)O(3)/Al2O24 laminated composites. J. Mater. Process. Technol. **196**(1–3), 356–364 (2008)

Woodward, R.L.: A simple one-dimensional approach to modelling ceramic composite armour defeat. Int. J. Impact Eng. **9**(4), 455–474 (1990)

Yi, R.C., Yin, L.K., Wang, J.R., et al.: Study on the performance of ceramic composite projectile penetrating into ceramic composite target. Def. Technol. **13**, 299 (2017)

Zaera, R., Sánchez-Gálvez, V.: Analytical modelling of normal and oblique ballistic impact on ceramic/metal lightweight armours. Int. J. Impact Eng. **21**(3), 133–148 (1998)